

OPEN

DATA DESCRIPTOR

# Mapping global development potential for renewable energy, fossil fuels, mining and agriculture sectors

James R. Oakleaf<sup>1</sup>, Christina M. Kennedy<sup>1</sup>, Sharon Baruch-Mordo<sup>1</sup>, James S. Gerber<sup>2</sup>, Paul C. West<sup>2</sup>, Justin A. Johnson<sup>3</sup> & Joseph Kiesecker<sup>1</sup>

Mapping suitable land for development is essential to land use planning efforts that aim to model, anticipate, and manage trade-offs between economic development and the environment. Previous land suitability assessments have generally focused on a few development sectors or lack consistent methodologies, thereby limiting our ability to plan for cumulative development pressures across geographic regions. Here, we generated 1-km spatially-explicit global land suitability maps, referred to as “development potential indices” (DPIs), for 13 sectors related to renewable energy (concentrated solar power, photovoltaic solar, wind, hydropower), fossil fuels (coal, conventional and unconventional oil and gas), mining (metallic, non-metallic), and agriculture (crop, biofuels expansion). To do so, we applied spatial multi-criteria decision analysis techniques that accounted for both resource potential and development feasibility. For each DPI, we examined both uncertainty and sensitivity, and spatially validated the map using locations of planned development. We illustrate how these DPIs can be used to elucidate potential individual sector expansion and cumulative development patterns.

## Background & Summary

Human activities have transformed most of the world’s terrestrial landscapes<sup>1</sup>, resulting in accelerated resource exploitation, environmental deterioration, biodiversity loss, and climate change<sup>2–4</sup>. Growing human populations<sup>5</sup> and increasing wealth in many regions<sup>6</sup> will inevitably propel further development to meet the rising demands for food, water, energy, and other land-based resources. Predicting and managing forthcoming development is essential to minimize the impacts of large-scale expansion on natural habitats and their services and to promote ecological and socioeconomic sustainability<sup>7</sup>. Anticipating where future development may occur requires mapping of land that is suitable to human activities<sup>8</sup> (e.g., growing crops, expanding housing development, establishing a mine), often taking into consideration the area’s biophysical criteria (e.g., prevailing climate, soil, topography), land use or administrative constraints (e.g., compatible land types, protected areas), and/or socio-economic factors (e.g., accessibility to markets or infrastructure) that are associated with the target development<sup>9,10</sup>.

Global land suitability mapping has aided our understanding of the expansion of many development sectors, including cropland or biofuel expansion, renewable energy sources (i.e., solar, wind, and hydropower), fossil fuels, and mining. However, previous global assessments for food and biofuel suitability are largely binary maps for “croplands” (e.g.<sup>11–13</sup>) or focus on marginal and abandoned land potential for biofuel production (e.g.<sup>14,15</sup>). A few cropland assessments account for social or policy constraints (e.g.<sup>13,16</sup>), but none globally map feasibility of land conversion based on factors of yield potential and access to infrastructure to distinguish relative conversion pressure<sup>8</sup>. Global mapping of renewable energy potential maps have incorporated only simple land constraints<sup>17–19</sup> or select few spatial development feasibility factors (e.g., market accessibility that considers distance to urban areas, load centers, and transmission lines<sup>20–24</sup>, or site construction and operational costs<sup>21,24,25</sup>), at times

<sup>1</sup>Global Lands Program, The Nature Conservancy, Fort Collins, CO, 80524, USA. <sup>2</sup>Global Landscapes Initiative, Institute on the Environment, University of Minnesota, St. Paul, MN, 55108, USA. <sup>3</sup>Natural Capital Project, Institute on the Environment, University of Minnesota, St. Paul, MN, 55108, USA. These authors contributed equally: James R. Oakleaf and Christina M. Kennedy. Correspondence and requests for materials should be addressed to J.R.O. (email: [joakleaf@tnc.org](mailto:joakleaf@tnc.org))

doing so only post-hoc to categorize potential energy production<sup>26,27</sup> or to compare implementation costs<sup>23,24</sup>. Global fossil fuels and mining sectors maps have been limited to one fuel or mineral type<sup>28–31</sup>, do not include spatial siting factors<sup>20,32</sup>, or rely on proprietary industry data that limits public distribution<sup>33</sup>. The inconsistency in mapping across different sectors and the lack of publicly available maps at resolutions finer than large-scale aggregate summaries (e.g., countries) severely limits the ability to plan for cumulative development pressures across geographic regions.

Here, we generated spatially-explicit, global land suitability maps at a fine resolution (1-km) for renewable energy (concentrated solar power – CSP, photovoltaic solar power – PV, wind power – Wind, and hydropower – Hydro); fossil fuels (coal mining – Coal, conventional oil – CO, conventional gas – CG, unconventional oil – UO, and unconventional gas – CG); mining (metallic minerals – MM and non-metallic minerals – NMM); and agriculture (crop expansion – Crop and biofuels expansion – Bio) development using publicly available datasets that account for both resource potential and development feasibility<sup>34</sup>. For each of the 13 sectors, we produced a land suitability index, referred to as a “development potential index” (DPI), that relatively ranks each 1-km area of land for its likelihood to be modified in the future by that sector and then classified each sector consistently on a high-low scale based on its DPI values. The sector-specific DPI datasets are made freely and publicly available to the scientific community and to policy decision-makers to facilitate broad-scale spatial assessments of potential individual sector and cumulative development patterns, and can be used to identify high-risk areas where near-future expansion may conflict with biodiversity, climate, or environmental assets.

We created DPIs using three main steps of spatial multi-criteria decision analysis (MCDA) techniques in geographic information systems (GIS) (Fig. 1)<sup>9</sup>. First, we mapped sector-specific land constraints expected to restrict development (e.g., suitable land cover, slope). Second, we produced spatially-explicit, independent criteria that were continuously-scaled factors that enhanced the suitability of sector development<sup>35</sup>, and captured both resource availability (sector-specific yields) and development feasibility (e.g., distance to major roads, railroads, ports, power plants, electrical grid, and demand centers). We removed areas with constraints from the mapped resource yield and development feasibility criteria and standardized values from 0–1. Third, we weighted the importance of spatial criteria using Analytic Hierarchy Process (AHP)<sup>36–38</sup>, and combined them into DPI maps using Weighted Linear Combination (WLC) in GIS<sup>9</sup>. We analyzed both output uncertainty and input sensitivity following refs<sup>39,40</sup> and validated our DPIs using over 6,000 points and 200,000 km<sup>2</sup> of mapped locations identifying recent or planned development sectors. While GIS within MCDA procedures (GIS-MCDA), specifically AHP in combination with WLC, have been widely used to map land suitability at local and regional scales<sup>10,41</sup> (e.g., siting of renewable energy facilities<sup>42–46</sup>, fossil fuel development<sup>47–49</sup>, mineral extraction<sup>50</sup>, and agriculture development<sup>51–53</sup>), to our knowledge, this is the first study to apply these procedures consistently across multiple energy, extractive, and agricultural sectors on a global scale.

## Methods

To inform parameters and criteria selection for each step of the analysis, we conducted a literature review of studies on the mapping of land suitability, yield potential, and/or economic feasibility associated with all development sectors (Online-only Table 1). Because technologies in all development sectors are rapidly changing, we limited our literature search to papers published within the last 10 years focusing mainly on global<sup>17–25,27,32,54</sup> and regional<sup>16,55–60</sup> analyses but also using state/local analyses<sup>44–51,53,61–66</sup> to fully capture the variety and weights of criteria used in all analyses. We relied on the most commonly cited development constraints and criteria that could be mapped from publicly available, open access global data to produce our DPI maps and thus facilitate public distribution of derived datasets.

Analyses were performed at a 1-km resolution for terrestrial lands defined as cells containing one or more 300-m pixels of terrestrial land cover types based on ESA CCI dataset<sup>67</sup>. We projected input data to the equal-area Mollweide projection and applied bilinear resampling method for continuous raster data and nearest-neighbor method for discrete data (vector data were first projected and then converted to raster datasets). Unless otherwise specified, analyses were conducted using ArcGIS 10.5 ([www.esri.com](http://www.esri.com)) with the Spatial Analyst 10.5 extension.

**Mapping development constraints (step 1).** Constraints were tied to resource thresholds (e.g., solar irradiance, wind speed), land use characteristics (e.g., urban areas), and biophysical characteristics (e.g., slope, elevation) that limit the ability of the sector to economically produce its associated commodity or to be constructed. Addition of these spatial constraints improved each sectors’ DPI by limiting the extent of the analysis to only viable locations<sup>16</sup>. Given the wide-range of constraints and their values often reported in the literature, we selected the least-restrictive constraint values reported by global or regional studies (see Online-only Table 1) to avoid the exclusion of areas that may become accessible to future development with improved technology. We did not include any administrative constraints (e.g., excluding protected areas) because these assignments can be modified or removed based on policy changes and land use pressure<sup>68</sup>. Online-only Table 2 provides sector-specific breakdown of the constraints applied with appropriate citations with their justifications, which we summarize briefly below.

For solar and wind renewable energy sectors (CSP, PV, Wind), we excluded areas below sector-specific resource (solar irradiance or wind speed) and above slope or elevation thresholds, and areas categorized as snow, ice, or urban. For CSP, we also excluded areas with already operating CSP power plants, and for wind, we excluded areas with  $\geq 3$  wind turbines per km<sup>2</sup> (we did not exclude existing PV power plants given lack of global data). For Hydro, we excluded urban areas, and locations with existing hydroelectric dams or estimated to produce <1 MW of power.

We excluded lands classified as urban for all fossil fuel and mining sectors. For coal mining, we also excluded existing coal mines based on our mapping from global sources, and for mineral and non-mineral mining, we excluded lands with former or current active mines. We did not exclude current oil and gas wells due to the lack

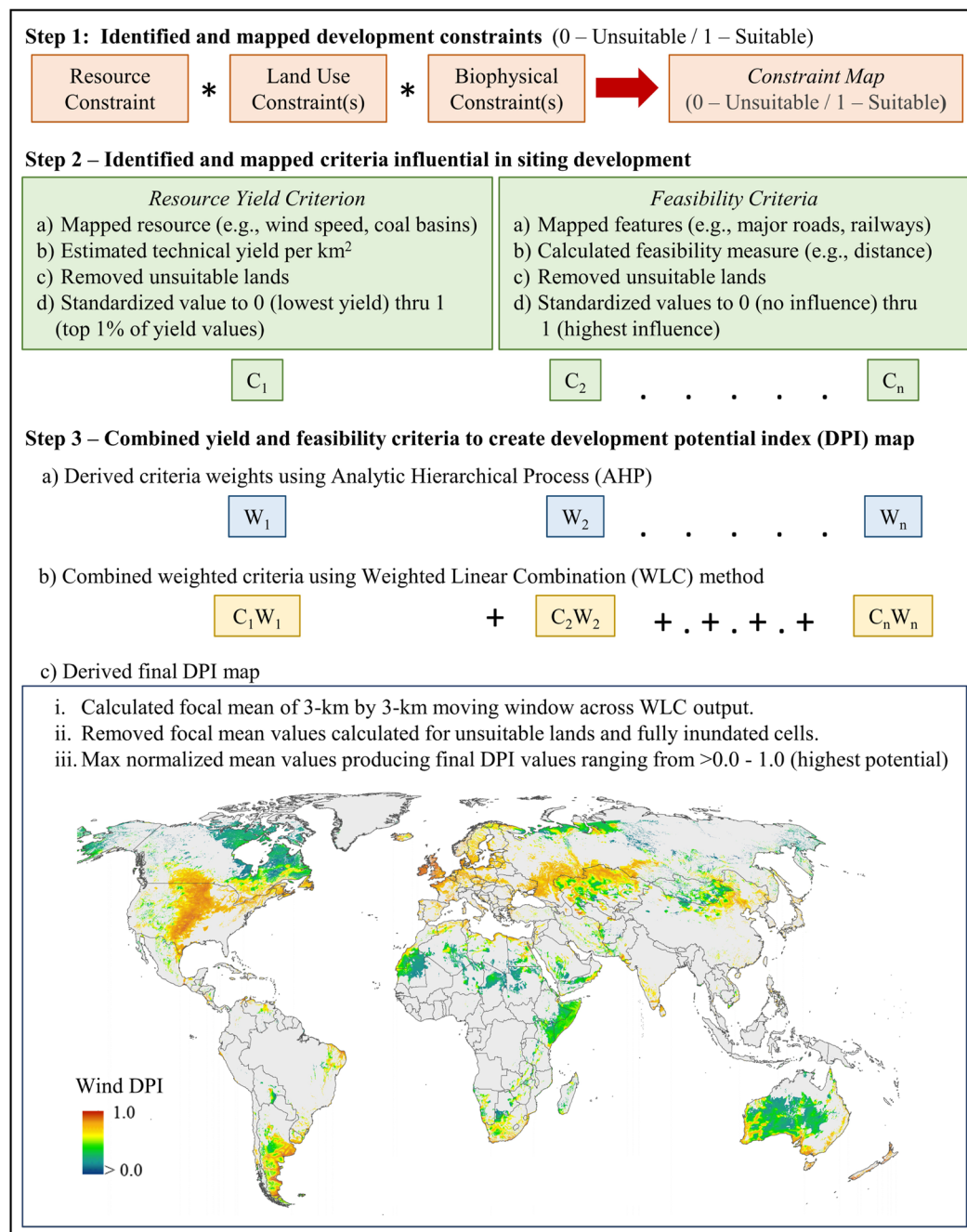


**Fig. 1** Procedures used to produce all development potential index (DPI) maps. Analysis steps were applied for the 13 sectors related to renewable energy, fossil fuels, mining, and agriculture.

of publicly available, globally comprehensive data on well locations. Lastly, for agriculture sectors, we removed lands classified as urban or currently cropped, arid lands without irrigation, and areas too steep for cultivation.

**Mapping development criteria (step 2).** *Mapping resource yield criteria.* For each sector, we spatially mapped a resource yield criterion based on available resources converted to yield estimates using common production values (e.g., annual megawatt hours, barrels of oil, tons of coal) for each 1-km<sup>2</sup> cell. See Online-only Table 2 for detailed methods and data applied to derive these resource yield maps with brief descriptions below. We limited the resultant global maps to suitable locations based our constraint maps (step 1), and applied the following steps on the yield map values to produce approximately normally distributed values ranging from 0–1 across all sectors: (1) reassigned values of cells that were within the top one percentile outliers to the 99<sup>th</sup> percentile value of the distribution, (2) applied transformation based on the skewness ( $s$ ) of the yield value distribution as follows: no transformation if  $s < 0.5$ , square-root transformation for  $0.5 \leq s \leq 1.0$ , and log-transformation if  $s > 1$ <sup>69,70</sup>, and (3) scaled data into a 0–1 range using min-max normalization. This approach addressed the right

skewed distribution of most yield cell values and maintained all cells but treated the top 1% of outlying yield values as a constant value given their expected lack of differentiation in development potential.

**Renewable energy:** We estimated yield for four renewable energy sectors: CSP, PV, Wind, and Hydro (Online-only Table 2). For solar (CSP and PV) and wind, we used the general equation:  $PD \cdot CF_i \cdot 8760$  to estimate annual yield (MWh/km<sup>2</sup>), where  $PD$  is the sector-specific power density in MW/km<sup>2</sup>,  $CF_i$  is the sector-specific and spatially explicit (for the  $i$ th cell) capacity factor derived from the corresponding resource estimate (e.g., wind speed for wind) and defined as the ratio of expected to potential power output, and 8760 is the number of hours in a year<sup>26,57,59</sup>. For wind, we multiplied this equation by a spatially-explicit air density factor ( $AD_i$ ), because differences in elevation have known effects on wind power production<sup>17,27</sup>. For hydropower, we used a publicly available, 1-km resolution hydropower potential dataset which derived potential from a global digital elevation model and river runoff data using a fixed  $CF$  value of 0.5<sup>18</sup>.

**Fossil fuels:** We estimated yield for five fossil fuel energy sectors: Coal, CO, CG, UO, and UG (Online-only Table 2). Yields were derived from global and national level assessments of technically recoverable resources per basin (coal), assessment units (CO, CG, UO, and UG), or prospective areas (UO and UG), which are collectively referred to as assessment units (AUs). For each AU, we divided the total recoverable resource by the AU area, thereby producing an average yield/km<sup>2</sup> across the AU. Where AUs overlapped, we summed resource-specific (e.g., conventional oil) yield values before producing the final yield map.

**Mining:** Due to the variety of different minerals mined and the lack of global, basin-level estimates of technically recovered minerals for each, we relied on proxy yield values based on deposit locations for two collective categories of mining: metallic and non-metallic (Online-only Table 2). Mineral deposit data were publicly available for 167 minerals along with categorical size estimates of deposit amounts that were determined from attribute size descriptions (e.g., very large, large, medium, etc.). Given the availability of only categorical estimates and because deposit densities are widely used to estimate undiscovered deposits and potential recoverable amounts<sup>71,72</sup>, we relied on mining density as a surrogate for yield. We implemented kernel density (KD) methods<sup>73</sup> using Kernel Density tool in ArcGIS, and incorporated categorical deposit amounts as weights following ref.<sup>74</sup>. Kernels were centered on each deposit location and generated based on deposit size weights and on radii distances specific to metallic or non-metallic minerals. We then selected only cells with  $KD > 0.001$  deposits/km<sup>2</sup>, a minimum value used by ref.<sup>75</sup> and <https://www.openstreetmap.org/>. Because 82% of mineral deposits were located within the U.S., we created and standardized KD maps separately for the U.S. and non-U.S. regions before combining these two regions to produce each sector's final resource yield map.

**Agriculture:** We estimated agriculture yield for ten food crops, which captured 83% of total calorie production on croplands<sup>76</sup>, and for a subset of five first-generation biofuel crops, which comprised the majority of commercial biofuel production<sup>77</sup> and have the most growth potential based on market maturity and technological capacity<sup>78</sup> (Online-only Table 2). Using 2012 yield data summarized at national or sub-national jurisdictional units, and following methods in ref.<sup>79</sup>, we modeled the crop-specific relationships between area-weighted yield (ton/km<sup>2</sup>) and biophysical covariates (e.g., growing degree-day, precipitation, fraction irrigated, slope, etc.) using a 95th percentile quantile regression to predict attainable yields (quantreg package version 5.33 in R version 3.4.0; model coefficient results in Online-only Table 3). We then combined spatially-explicit covariate maps with the resulting model coefficients to produce global, crop-specific, predicted yield maps. For crop expansion, we min-max normalized these yield values for each crop. For biofuel crops, we converted predicted yield in ton/km<sup>2</sup> to gallons of gasoline equivalents (GGE) per km<sup>2</sup> based on conversion rates from ref.<sup>20</sup>. We generated final cropland and biofuel resource potential maps by calculating the mean standardized yield value (i.e., 0–1 for crops and GGE/km<sup>2</sup> for biofuels) across the ten subsistence crops and five biofuel crops respectively, and then ensured normal distribution of these two final yield maps following the methods discussed previously.

**Mapping feasibility criteria.** We produced 13 development feasibility criteria at 1-km resolution, which were factors that increase site development potential or decrease operational costs (details in Online-only Table 4). These criteria related to: (1) ability to transport resources and/or construction materials (distance to major roads, railways, and ports); (2) access to resource demand centers (market accessibility, distance to the electrical grid, urban areas, coal-fired power plants, and aggregate demand centers); (3) locations of existing development (distance to producing oil and gas fields and active coal mining density); and (4) other economic costs associated with resource siting (inverse population density), development (landcover feasibility and land supply elasticity), and/or production (access to electricity). Criteria values ranged from 0 to 1, with 1 indicating the most preferred location for a particular sector development associated with the criteria, and 0 implying the criteria no longer provided any advantage for this development. For each sectors' MCDA, we selected criteria used in previous studies on land suitability or recognized as an economic factor influencing siting (Online-only Table 1), and that could be mapped globally from existing, publicly available data.

We generated distance criteria values ( $c$ ) based on a Gaussian distance decay function,  $c = \exp(-d^2/2 \cdot (h/2)^2)$ , where  $d$  is Euclidian distance between a focal cell and the closest feature of influence (e.g., transmission line, roads, railway, etc.), and  $h/2$  is the inflection point, or the point beyond which the criteria score starts to rapidly decline towards zero. Resulting standard values of  $c$  ranged from 0–1, where 1 indicated closest proximity to the feature of importance. For renewable energy sectors, we set  $h$  to 100 km similar to ref.<sup>56</sup>, and for fossil fuels and mining sectors, we set  $h$  to 50 km, or the average distance at which infrastructure costs associated with mineral extraction approximately doubles<sup>80</sup>.

**Combining yield and feasibility criteria to create DPis (step 3).** We used Analytic Hierarchy Process (AHP)<sup>36,81</sup> and Weighted Linear Combination (WLC)<sup>9</sup> methods to combine resource yield and feasibility criteria maps into a final DPI map for each sector. AHP calculates criteria weights from a pairwise matrix of importance values (judgement matrix) formulated based on scaled rankings<sup>36,37</sup>. Pairwise comparison values are assigned

DPI Class	Standard z-score range*	Estimated percentile range*
Very High	>1.282	>90 <sup>th</sup> percentile
High	0.675–1.282	75 <sup>th</sup> percentile–90 <sup>th</sup> percentile
Medium-high	0.000–0.675	50 <sup>th</sup> percentile–75 <sup>th</sup> percentile
Medium-low	–0.675–0.000	25 <sup>th</sup> percentile–50 <sup>th</sup> percentile
Low	–1.282––0.675	10 <sup>th</sup> percentile–25 <sup>th</sup> percentile
Very Low	<=–1.282	<=10 <sup>th</sup> percentile

**Table 1.** Development potential index (DPI) classes. Standard z-score ranges used to define Development Potential Index (DPI) classes and estimated percentile data ranges based on normally distributed values. \*Highest value in range included in class (e.g. z-score 1.282 is assigned to High DPI class).

based on Saaty's nine-point importance scale<sup>36,37</sup>, where a score of 9 indicates criterion A is nine times more important than criterion B, and where scores are reciprocal (therefore criterion B is 1/9 times as important as criterion A). We selected criteria, none of which were highly correlated (Pearson's correlation > 0.6) and assigned importance values based on our literature review of sector suitability (Online-only Table 1), current literature on resource transportation and development costs<sup>80,82–113</sup>, and authors' expertise. Criteria weights were calculated as the normalized eigenvector associated with the judgement matrix's largest eigenvalue ( $\lambda_{max}$ ) (see refs<sup>36,37</sup> for details). We evaluated the consistency of the judgement matrices using a consistency ratio (CR) calculated as  $CR = CI/RI$ , where  $CI$  is the consistency index calculated based on number of criteria ( $n$ ) as  $CI = (\lambda_{max} - n)/(n - 1)$ , and  $RI$  is an established random inconsistency index based on  $n$  (see Table 1.2 in ref.<sup>81</sup>).

We found all judgment matrices to be within acceptable consistency (i.e., CRs < 0.10). For all judgement matrices, the resource yield criterion was identified as the most important, which produced weight ranging from 0.336 (coal) to 0.552 (metallic mining). Judgement matrices of fossil fuel sectors included feasibility criteria related to current development, which were prioritized as next highest, or equal to, resource yield criteria. For all other sectors, the typical second highest prioritized criteria were related to transporting the resource to its respective demand centers, except for hydropower, for which population avoidance (i.e., inverse population density criterion) ranked as second highest. Supplementary Table S1 provides judgement matrices for each sector including justifications for importance ranking, and derived weights used to calculate DPIs.

Once we derived the resource yield and feasibility criteria maps with their associated weights, we implemented WLC in ArcGIS using the Weighted Overlay tool to create sector-specific DPI maps using:  $\sum w_n c_n$ , which produces a composite DPI map based on AHP derived weights ( $w_n$ ) for  $n$  criteria ( $c_n$ )<sup>9</sup>. Values of all input criteria maps and resulting DPI maps ranged from >0 (low) to 1 (high). To reduce local variations as a result of global data inaccuracies or resolution artifacts, we spatially averaged DPI values using a  $3 \times 3$ -km moving window analysis<sup>10</sup>. If any cell previously excluded based on constraints or water was assigned a value by the smoothing technique, we reassigned its value to null. A final continuous DPI was created by max normalizing the remaining spatially-averaged values<sup>34</sup> (e.g., Fig. 1-Step 3iii).

**DPI classification.** To facilitate the comparison of spatial patterns across the different sectors, we grouped the continuous DPI values into six relativized development potential classes: very high, high, medium high, medium low, low and very low. Given that each sector's DPI values were approximately normally distributed but varied in their mean values, we calculated the standard global z-score per pixel and then binned each DPI based on five z-score breakpoints that corresponded to the percentiles of the distribution (Table 1). This method classified each DPI equally based on its mean and standard deviation of values using consistent estimated percentage breakpoints of 10% (Very Low, Very High), 15% (Low, High), and 25% (Medium-high, Medium-low). These breakpoints are offered as one way to classify the continuous DPI values and are included in each sector-level DPI data bundle<sup>34</sup> (e.g., Supplementary Table S1). We note that these six classes have been applied in previous global threat analyses (e.g., by ref.<sup>114</sup> when classifying cumulative threats to global marine environments).

**Uncertainty and sensitivity analyses.** For each DPI sector, we quantified the variability associated with each output based on model input (i.e., uncertainty analysis), and then identified which DPI criteria were responsible for the most variability (i.e., sensitivity analysis).

**Uncertainty analysis.** The two main sources of uncertainty for any MCDA arise from the criteria maps and their weights<sup>9,115</sup>. For the criteria maps, uncertainty can stem from three aspects in the analysis; (1) choice of criteria in the decision model, (2) errors of measurement in the original source spatial data, and (3) the value scaling (or standardization) of the criterion maps<sup>115</sup>. To reduce these sources of uncertainty, we respectively (1) relied on supported literature to guide criteria selection and value scaling of categorical data (Online-only Table 1), (2) avoided arbitrary classifications of continuous input data, and (3) applied fuzzy measures when appropriate. We focused our uncertainty analysis on the weighting values, a common approach when addressing uncertainty regarding GIS-MCDA<sup>39,116–118</sup>. To do so, we relied on a Monte Carlo (MC) approach, which assesses both qualitative and quantitative uncertainty within an MCDA based on repeated random sampling from a range of criteria weights to produce several iterations of the model results<sup>118</sup>. These iterations are then used to calculate standard deviation (SD) and/or coefficient of variation (CV) to map and analyze uncertainty<sup>39,116,117,119</sup>.

DPI Sector	Mean CV	Number of Criteria in MCDA
Biofuels Expansion	0.1373	3
Crops Expansion	0.1076	3
Metallic Mining	0.0798	4
Non-metallic Mining	0.0701	4
Coal Mining	0.0664	6
Conventional Gas	0.0609	5
Unconventional Gas	0.0572	5
Conventional Oil	0.0527	5
Photovoltaic Solar Power (PV)	0.0480	6
Hydropower	0.0450	6
Concentrated Solar Power (CSP)	0.0439	6
Unconventional Oil	0.0415	5
Wind Power	0.0279	7

**Table 2.** Mean coefficient value (CV) for 13 development sectors with number of criteria used for each development potential index (DPI). Sectors ordered from largest to smallest mean CV.

To define our weight ranges for each DPI criterion, we modified the original AHP by first increasing the importance value of a selected criterion by two points across all other criteria and then used this new matrix to calculate the maximum weight for this criterion weight range. We then decreased the importance value for this same selected criterion by two points across all criteria to derive the minimum weight for the range. This process emulated selecting the next highest or lowest odd number comparison value (i.e., 1, 3, 5, 7, 9 values most commonly used when assigning values using the Saaty's nine-point importance scale<sup>36</sup>), while also maintaining the necessary consistency ratio (i.e.,  $CR < 0.1$ ) to use these derived weights (see the Supplementary Information for an example). Once the weight ranges for all criteria were defined (Online-only Table 5), we followed standard MC methodology and applied a four step process similar to refs<sup>39,120</sup> for each DPI. For 300 iterations, we: (1) randomly selected a criterion, (2) randomly assigned the criterion weight from its bracketed range of generated weights (Online-only Table 5), (3) proportionally modified the remaining criteria weights such that all weights sum to the value of one, and (4) applied these weights to reproduce the modified DPI. Our chosen number of 300 iterations falls within the recommended range of 100–10000<sup>121,122</sup> and predominantly produced a  $< 1\%$  change of the mean and SD associated with each iteration as the iterations neared 300 which suggested this number was sufficient<sup>117</sup>.

Based on mean CV across all DPI maps, the biofuel and crop DPIs exhibited the highest relative uncertainty, largely attributed to these DPIs having the lowest number of criteria (Table 2). In contrast, the wind DPI had the lowest uncertainty, likely driven by this sector having the greatest number of criteria. This inverse relationship between uncertainty and the number of criteria was upheld by all sectors except coal and unconventional oil (Table 2). Coal had higher than expected uncertainty presumably because of the larger undeveloped basins located in remote regions of the globe. Unconventional oil basins on the other hand are found in more accessible locations and consistently much smaller in size in comparison to other fossil fuel sectors; thus, limiting the variability caused by development feasibility criteria and thus also reducing uncertainty.

Similar to refs<sup>39,120</sup>, we classified all 13 CV datasets values into “Very Low” to “Very High” classes using the same DPI classification method based on z-score breakpoints<sup>34</sup> (6 classes; Table 1). For each sector, we determined the DPI class(es) that exhibited the greatest uncertainty by calculating the percentages of DPI classes within each uncertainty class (for 36 different combinations; e.g., Fig. 2). We also averaged percentages of the 36 combinations across all 13 DPIs for a comprehensive uncertainty measure (Fig. 3). None of the DPI cells classified as “Very High” or “High” were found to fall within “Very High” or “High” uncertainty classes (Fig. 3). Rather,  $>99\%$  “Very High” DPI cells and  $>75\%$  of “High” DPI cells fell within the “Low” or “Very Low” uncertainty classes, respectively. These results indicate less uncertainty exists in high DPI areas. In contrast, the areas with highest uncertainty (i.e., “Very High” and “High” classes) fell within the “Low” and “Very Low” DPI classes for most sectors. These high uncertainty areas tended to occur in remote regions that lacked supporting infrastructure or market access but had higher than average resource potential (i.e., yield criteria in all DPIs), especially for the renewable and fossil fuel sectors. However, this same spatial pattern was not as prevalent for mining and agriculture sectors, where the highest uncertainty values largely occurred in regions that had low yield but were farther from markets or infrastructure. Readers can further explore the spatial distributions of uncertainty across each DPI by downloading data from figshare<sup>34</sup>.

**Sensitivity analysis.** For each sector DPI map, we evaluated the sensitivity of the multi-criteria weights using a one-at-a-time (OAT) method: where we incrementally modified weights within a range of values and then compared the modified and original ( $DPI_{Orig}$ ) outputs<sup>9,41</sup>. Following ref.<sup>115</sup>, we varied weights  $-20\%$  to  $+20\%$  of original weight value in increments of  $\pm 2\%$  ( $n = 21$  simulation runs), and determined the change in cell counts within five DPI value bins (i.e.,  $>0.0-0.2$ ,  $>0.2-0.4$ ,  $>0.4-0.6$ ,  $>0.6-0.8$ ,  $>0.8-1.0$ ). These five, equal interval bins were used to evaluate the sensitivity across the spectrum of continuous DPI values to distinguish changes in consistent value ranges across sensitivity runs while also reducing computing resources needed for a per pixel measurement. For each criterion and its bins, we calculated the average percent change in cell counts relative

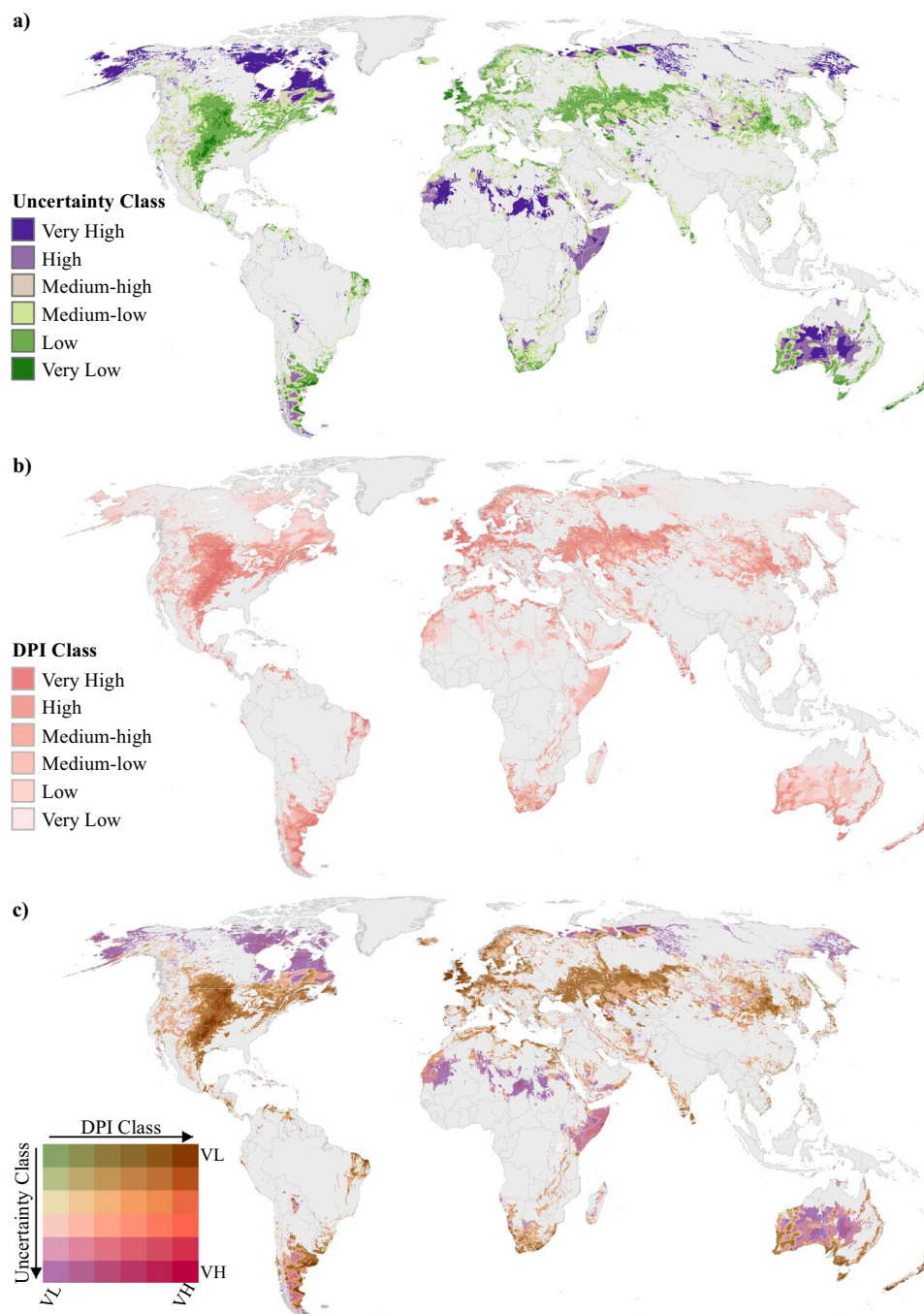


**Fig. 2** Example spatial uncertainty analysis for wind development potential index (DPI). Spatial datasets used for wind DPI uncertainty analyses: **(a)** classified wind uncertainty map, **(b)** classified wind DPI map, and **(c)** resulting map produced by intersection of two maps. In the legend for map **(c)**, arrows indicate the direction of classes going from “Very Low” (VL) to “Very High” (VH). For example, purple areas classified as VL for DPI and VH for uncertainty, whereas dark brown areas classified as VH for DPI and VL for uncertainty. Non-classified areas are identified in grey and were excluded based on a lack of available future resources or by constraints applied during the DPI analysis.

to the counts from  $DPI_{Orig}$  (Online-only Table 6). We additionally evaluated the spatial differences in outputs by calculating the cell-based correlations (Pearson’s  $r$ ) between the modified DPI outputs and  $DPI_{Orig}$ . Detailed sensitivity reports that included the percentage change per bin per simulation run for all sector criteria and the corresponding correlations are packaged with individual DPI data bundles<sup>34</sup>.

Unsurprisingly, the most sensitive criteria were the highest weighted ones and the least sensitive criteria were the lowest weighted ones across all DPis. The most sensitive criterion was resource yield for all sectors, except for coal, for which mining density (equally weighted as coal resource yield) was the most sensitive. The least sensitive criteria were distance to railways or ports (CSP, PV, CG, UO, UG, NMM), distance to major roads (CO), distance

		DPI Class						
		Very Low	Low	Med-low	Med-high	High	Very High	
Uncertainty Class	Very Low	0.02%	0.06%	0.18%	0.47%	1.47%	6.88%	9.08%
	Low	0.10%	0.21%	1.00%	4.75%	12.28%	3.25%	21.59%
	Med-low	0.38%	1.15%	4.43%	10.23%	3.45%	0.28%	19.92%
	Med-high	1.30%	4.28%	12.13%	5.31%	0.44%	0.03%	23.49%
	High	2.66%	6.62%	5.66%	0.57%	0.00%	0.00%	15.51%
	Very High	5.92%	3.99%	0.51%	0.02%	0.00%	0.00%	10.44%
		10.38%	16.31%	23.91%	21.35%	17.64%	10.44%	(total DPI percentages)

**Fig. 3** Cross tabular average percentages of development potential index (DPI) classes in each corresponding uncertainty class. Data for each DPI and uncertainty class were averaged across all 13 sectors and total percentages are summarized at the bottom (total percentage in DPI class) and right (total percentage in uncertainty class) of the table. Six colors classify percentages from lowest to highest (i.e., light-blue [0%], light-green [0–1%], yellow [1–3%], light-red [3–5%], red [5–7%], and dark-red [ $>10\%$ ]).

DPI Sector	Criteria with greatest variability in high DPI bins	Sensitivity run with greatest change	Maximum absolute change from $DPI_{Orig}$ cell values	Average absolute change from $DPI_{Orig}$ cell values	Maximum absolute change from $DPI_{Orig}$ cell values $> 0.5$	Average absolute change from $DPI_{Orig}$ cell values $> 0.5$
Coal	Active coal mining density	–20%	0.066	0.036	0.066	0.049
Hydro	Resource yield	–20%	0.091	0.039	0.091	0.023
Wind	Resource yield	–20%	0.087	0.026	0.087	0.023

**Table 3.** Sensitivity analysis results summarized as change in DPI values. Sector-specific maximum and average absolute change in cell values from  $DPI_{Orig}$  cells (all cells and cells  $>0.5$ ) to DPI cells produced by the sensitivity run with the maximum weight change (i.e., +20% or –20%). Data are presented only for sectors that exhibited the greatest variability in the high DPI bins, i.e., 4 ( $>0.6–0.8$ ) and 5 ( $>0.8–1.0$ ). Abbreviations of sector are as follows: Coal – coal mining, Hydro – hydropower, and Wind – wind power.

to urban areas (Wind, Hydro), or distance to coal power plants (Coal). Overall, biofuels DPI exhibited the greatest sensitivity due to high shifts in the lowest bin ( $>0–0.2$ ) (Online-only Table 6; see additional details below).

For most criteria and sectors, the lowest bin ( $>0.0–0.2$ ) exhibited the greatest sensitivity, likely because it had the smallest overall frequency of cells within the  $DPI_{Orig}$ , and thus the greatest percent changes. To focus on high development potential areas that are most influential to predicting land expansion areas, we examined the sensitivity exhibited within the top bins. For the second highest bins ( $>0.6–0.8$ ), the most sensitive criterion within any sector-MCDA was coal mining density followed by hydropower resource yield. For the top bin ( $>0.8–1$ ), the resource yield criterion for wind exhibited the greatest shifts. To further examine the sensitivity of these three criteria, we calculated the maximum and average absolute cell value change on a cell by cell basis associated with the sensitivity run having the greatest degree of change for all cell values and for cells with  $DPI_{Orig}$  values  $> 0.5$ . Even for the sensitivity runs with the greatest weight change (i.e., +20% or –20%), the maximum absolute cell change was less than 0.1 and the average absolute change was less than 0.05 across all cells and for  $DPI_{Orig}$  cells that were greater than 0.50 (Table 3, see Supplementary Fig. 1 for mapped example with Coal DPI).

Overall across all sectors, the binned value of most cells remained the same, and there were no cells that either increased or decreased more than one bin level from that of the original run. Furthermore, spatial correlations were  $r \geq 0.971$  for all sensitivity runs across all sectors, indicating low spatial variance in the DPI outputs due to modified weights. An overall low sensitivity was further reinforced by an only slight change (i.e.,  $\sim 0.05$ ) detected in cell values for the three most sensitive sector criteria when applying the maximum weight change.

### Data Records

For each development sector, three spatial datasets (i.e., the continuous DPI, the classified DPIs, and the classified uncertainty map) are accessible via figshare as GeoTIFF raster datasets at 1-km resolution using the Mollweide projection<sup>34</sup>. Due to large file sizes and for ease of access, all sector DPI data are bundled together within a correspondingly named zip file (e.g., Wind.zip). Each zip file contains: the continuous DPI raster dataset, the classified DPI raster dataset, the classified uncertainty raster dataset, all parameter descriptions and values (i.e., constraints, criteria correlations and weights, and AHP comparison values and matrix consistency ratio) used to produce the DPI, along with the full DPI sensitivity report. Additionally, four zip files (i.e.,



Recent and Potential Development Data	Data Type	Data Spatial Extent	Sample Size	DPI Overlap (% total)						
				Very high	High	Med- high	Med- low	Low	Very low	None
CSP Plants <sup>123</sup>	Points	North America	5	4 (80%)	0 (0%)	0 (0%)	0 (0%)	0 (0%)	0 (0%)	1 (20%)
PV Plants <sup>123</sup>	Points	North America	2,238	124 (6%)	488 (22%)	1,446 (64%)	115 (5%)	1 (0%)	0 (0%)	65 (3%)
Large PV Plants <sup>123</sup> (i.e., capacity >=20 MW)	Points	North America	483	71 (15%)	173 (36%)	225 (47%)	13 (3%)	0 (0%)	0 (0%)	1 (0%)
Wind Farms <sup>123</sup>	Points	North America	411	175 (43%)	171 (42%)	37 (9%)	2 (0%)	1 (0%)	0 (0%)	25 (6%)
Hydropower <sup>124</sup>	Points	Global	2,231	457 (20%)	511 (23%)	637 (29%)	316 (14%)	169 (8%)	141 (6%)	NA
Large Hydropower <sup>124</sup> (i.e., capacity >=30 MW)	Points	Global	946	284 (30%)	197 (21%)	233 (25%)	140 (15%)	51 (5%)	41 (4%)	NA
Coal Permits <sup>126</sup>	Polygons	US	10,848 km <sup>2</sup>	9,458 (87%)	805 (8%)	126 (1%)	0 (0%)	0 (0%)	0 (0%)	459 (4%)
Oil and Gas Leases <sup>125</sup>	Polygons	Western US	74,150 km <sup>2</sup>	32,304 (44%)	17,305 (23%)	18,404 (25%)	2,496 (3%)	120 (0%)	0 (0%)	3,521 (5%)
Mining Claims <sup>125</sup>	Polygons	Western US	42,392 km <sup>2</sup>	15,430 (36%)	14,601 (35%)	9,675 (23%)	2,209 (5%)	188 (0%)	51 (0%)	256 (1%)
Crop Expansion <sup>127</sup>	Pixels	Contiguous US	83,686 km <sup>2</sup>	23,819 (29%)	22,508 (27%)	15,399 (18%)	7,688 (9%)	5,941 (7%)	1,960 (2%)	6,371 (8%)

**Table 4.** Spatial validation of DPI maps. The percentage of overlap between mapped DPI classes and recent and potential development locations with information on data type, spatial extent, and sample sizes.

DPI\_Inputs\_and\_Scripts\_Part01-04.zip) are provided and contain all input data and Python scripts necessary to reproduce any DPI<sup>34</sup>. All three raster datasets per sector can also be viewed and examined interactively at [http://s3.amazonaws.com/DevByDesign-Web/Maps/DPI\\_viewer/index.html](http://s3.amazonaws.com/DevByDesign-Web/Maps/DPI_viewer/index.html).

### Technical Validation

To validate the DPIs, we used spatial point locations of planned or recently developed renewable energy power plants<sup>123,124</sup>, recent lease and claim boundaries identifying where fossil fuels and mining development is permitted<sup>125,126</sup>, and recent areas of crop expansion<sup>127</sup>. We compared mapped DPI classes to recent or planned development locations and determined the percentage of overlap and non-overlap (“none” class; Table 4).

For solar power plants and wind farms, we used the most comprehensive database on recently developed or planned development locations<sup>123</sup>; data were only available for North America. We included records with available x/y coordinates (i.e., not city or county) for facilities constructed no earlier than 2016 or that were currently planned (see Table 4 for sample sizes). We assigned a DPI class value for each point based the closest DPI classified cell that fell within a maximum distance representing the square-root of the mean facility-area reported for the sector. For example, CSP plants average 6.64 km<sup>2</sup> in size<sup>128</sup>, so we assigned the DPI class of the nearest cell within 2.58 km (i.e., square-root of 6.64), otherwise the location was classified as not having a class (i.e., None). We used a distance threshold of 1.77 km for PV based on ref.<sup>128</sup> and 7.35 km for wind based on ref.<sup>129</sup>. We found that all but one of the CSP plants fell within the very high DPI class (Table 4). The vast majority of utility-scale PV power plants (92%) and all but 13 of the large PV plants (i.e., >=20 MW, cutoff identified by ref.<sup>128</sup>) fell within very high, high, or medium-high DPI classes (Table 4). Similarly, 85% of all wind farms fell within our mapped high and very high DPI areas and only twenty-five sites (6%) fell outside of any DPI class. For hydropower, we relied on the a dataset that identified proposed and currently constructed hydropower dams globally<sup>124</sup>. Because there were no feature-level location error assessments (i.e., how accurately each dam location was mapped), we only used future dam sites which were within 1 km of any DPI category cells. We found that 72% of all dam locations and 76% of large hydropower dams (i.e., >30 MW, cutoff identified by ref.<sup>130</sup>) fell within medium-high to very high DPI classes.

For coal, we used a U.S. coal mining permit database<sup>126</sup> (n = 4,650 permits), that maps boundaries where companies have the right to disturb land for the mining and will be required by law to reclaim the site. Based on intersecting these lease boundaries with mapped DPI classes, we found that 87% of permit areas not mined fell within the highest DPI (only 4% were outside of any DPI cell). For oil and gas and mineral extraction sectors, we used a U.S. lease databases for oil and gas removal and mining claims<sup>125</sup>. Given the lack of publicly available data for these sectors and the high costs associated with more expansive proprietary data, we were limited to data within 10 western U.S. states: California, Oregon, Nevada, Idaho, Utah, New Mexico, Colorado, Wyoming, Montana, North Dakota, and South Dakota. Because oil and gas lease data did not distinguish the resource (i.e., oil or gas) or the method used (i.e., conventional or unconventional), we combined the DPI classes for CO, CG, UO, and UG and maintained the highest class per cell. We similarly combined metallic and non-metallic mining claims because these were not distinguished in the dataset. We overlapped oil and gas leases and mining claims with their associated combined DPI maps and found that >67% of oil and gas leases were located within very high or high DPI scores (only 5% were outside of any DPI cell), and 71% of mining claims not already mined overlapped with the two highest DPI classes (only 1% fell outside of DPI cells).

For cropland, we relied on spatial maps of annual cropland percentages per 1-km<sup>2</sup> within the conterminous U.S. over the past 150 years<sup>127</sup> and calculated the percentage of expansion for the most recent year of 2016 (i.e., we subtracted 2015 from 2016 percentages and selected only those cells with positive values). This identified over two million pixels (totaling 83,685.87 km<sup>2</sup>) with cropland expansion, which we overlapped with Crop DPI maps and calculated the total expansion per DPI class. We found that 73% of cropland expansion occurred in medium-high to very high DPI classes and over 46,000 km<sup>2</sup> (56%) occurred in the top two classes. We were unable to find an analogous biofuels expansion dataset but assert that these results offer indirect support given that the (1) the cropland expansion dataset includes all biofuel crops, and (2) our biofuels DPI was created from the yield potential of a subset of crops and the same feasibility criteria (i.e., market accessibility and land supply elasticity) as the cropland DPI.

### Usage Notes

The DPI maps generated here provide some of the first globally consistent land suitability maps at a fine resolution (1-km) that depict the potential expansion for 13 major development sectors related to renewable energy, fossil fuels, mining, and agriculture. Our approach offers an advancement to other products by factoring in resource yield potential alongside multiple spatial factors that influence development siting using a spatial MCDA approach. It also advances the global mapping of multiple energy and extractive sectors that increasingly play a role in land use change<sup>131</sup>, but have been overlooked relative to agriculture or urban expansion<sup>132,133</sup>. Further, we examined the uncertainty and the sensitivity of each DPI and validated results with the best available known locations of recent or planned development: efforts rarely performed even for site-based or regional land suitability analyses<sup>41</sup>.

We acknowledge that our DPIs, like all global data, are inherently prone to inaccuracies, omissions, and inconsistencies in both their spatial features and attributes. While we used the best publicly available and current data for our analyses, input datasets were not always comprehensive in regional coverage (an issue that plagues all global analyses); however, with the provided Python code, each DPI can be easily updated as new data becomes accessible. For example, because only proprietary, global pipeline spatial data were available, our oil and gas DPIs (i.e., CO, CG, UO, UG) lacked this important criterion in the analysis and instead we relied on distance to existing oil and gas fields as a proxy that identifies where pipelines exist. Additionally, our DPIs do not consider governmental actions (e.g., environmental regulations, incentives, tax breaks) that often influence development siting, and may not capture land expansion under varying market changes and technological advancements. Given the frequency of policy and market changes, variations across administrative units, and the effort required to maintain such a database, incorporating the above was beyond the scope of this study, but future work, especially if focused on a smaller focal area, should seek to capture these criteria and/or conditions to update DPIs. We also do not account for climate change, which has been shown to redefine future crop yields<sup>13</sup>, and has the potential to inundate areas of current suitable land and/or supporting infrastructure, relocate population/demand centers of resources, modify precipitation or cloud cover patterns that can alter hydropower and solar resources<sup>134,135</sup>.

Finally, we recognize there are multiple uncertainties throughout any MCDA process (e.g., setting constraints, calculating spatial criteria values, and selecting criteria weights), and we only evaluated the uncertainty and sensitivity of one primary source (criteria weights). Nevertheless, our DPI maps offer more detailed and consistent global products on the relative (rather than the precise) suitability of lands for future development expansion. Although we produced DPI maps at a 1-km resolution, we do not recommend the use of these data at this resolution for local land-use planning or siting of development. We provide the DPI maps at this resolution (1) given its consistency with the input spatial feasibility metrics; (2) because it allows for the aggregation of data into comparable zones of analysis (e.g., countries, states/provinces, ecoregions, watersheds, etc.) that circumvent the modifiable areal unit problem often introduced with coarse resolutions<sup>136</sup>; and (3) because it maximizes the potential discernment of spatial heterogeneity in global development patterns<sup>137</sup>. While our validation results produced favorable support of our products, we emphasize that more localized or detailed spatial MCDA analysis should be performed using much finer resolution and higher accuracy data to fully resolve land suitability at 1-km pixel level. In addition, feedback should be solicited from local decision makers, industry representatives, and sector specialists to select regionally-tailored criteria factors and assigning their influence (weights) on development in the analysis.

Despite these limitations, the timeliness and substantial need for these types of data are demonstrated by an increasing number of online portals hosting spatial data on human development pressure along with environmental features: e.g., the World Resource Institute's (WRI) Resource Watch (<http://resourcewatch.org>), the World Wildlife Foundation's (WWF) Sight (<http://wwf-sight.org/explore>), the European Commission Joint Research Center's Digital Observatory for Protected Areas (DOPA) (<http://dopa-explorer.jrc.ec.europa.eu/>), the Global Forest Watch (<http://www.globalforestwatch.org>), the United Nation's MapX (<http://www.mapx.org/>), the UN Biodiversity Lab (<https://www.unbiodiversitylab.org/about.html>), and the World Bank's Spatial Agent (<https://olc.worldbank.org/content/spatial-agent-tutorial>), among others. We note that the development pressure datasets hosted on these online portals predominately focus on current development patterns, thus, they are limited to retrospective or current planning efforts. Of the select datasets that capture potential future expansion areas, they tend to map only areas of unexploited resources (e.g., resource yield proxies) without integrating spatial feasibility factors. Figure 4 displays some of the representative resource datasets from the above sources in comparison with the most analogous DPIs from this study. Previous existing maps identify locations of resources without resource value attribution (Fig. 4e) or captures resource yield potential but without spatial details on siting constraints (i.e., Fig. 4a vs Fig. 4b) and/or siting feasibility (i.e., Fig. 4c vs Fig. 4d). In addition, these maps often only capture one segment of a sector thereby neglecting the overall sector development pressures (i.e., Fig. 4g vs. Fig. 4h). While current development maps delineate regions susceptible to single-sector expansion over the long-term and can

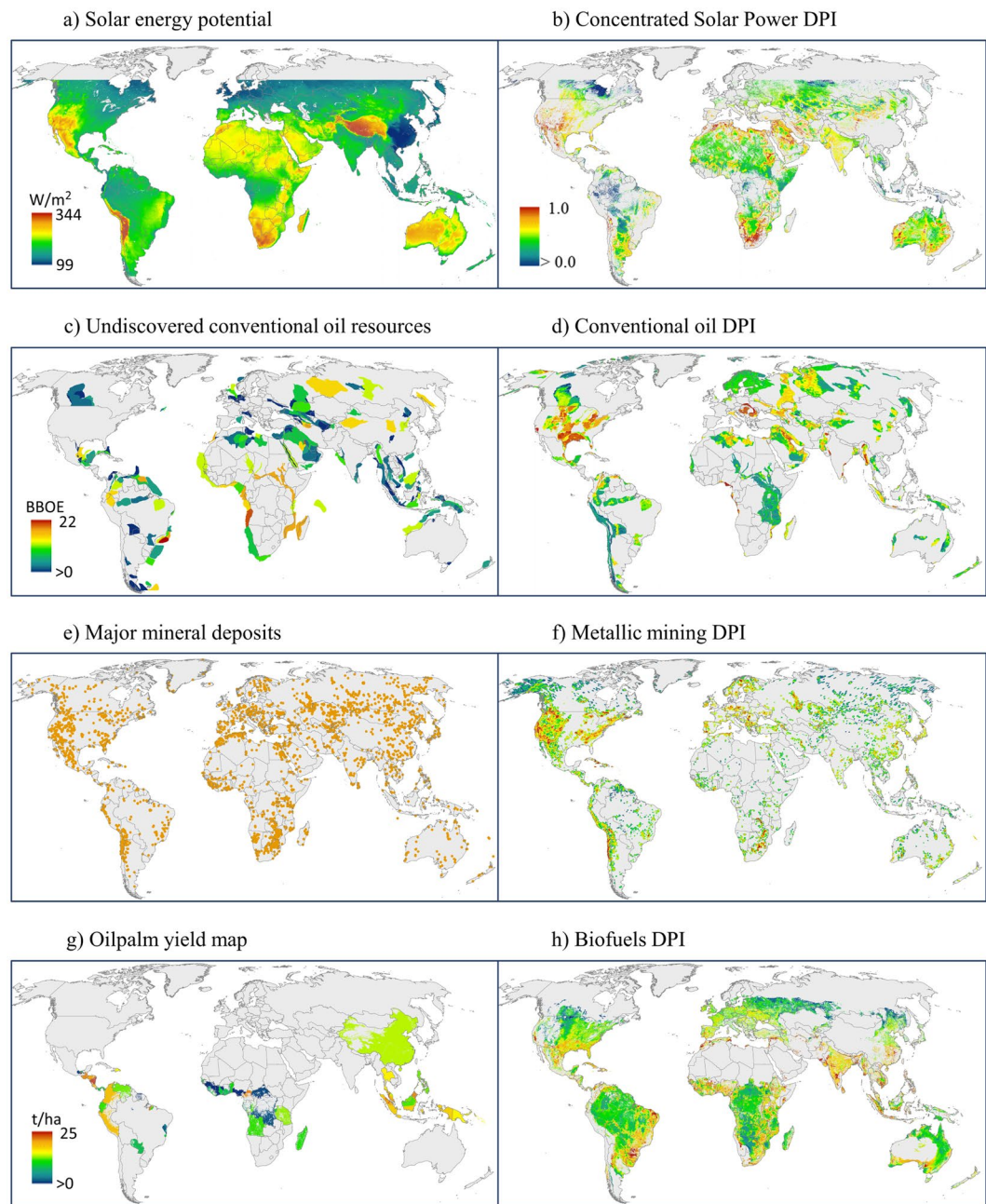


**Fig. 4** Comparison of DPs with publicly available resource data. Data on resources were obtained from WRI Resource Watch and partners (left side panel) with the most analogous DP maps produced by this study (right side panel). Color ramp for all maps are the same, with highest values in dark orange and lowest values in blue and null value in grey. Legend in first DP map (**b**) can be applied to all other DP maps (**d,f,h**). Map of only potential resource locations are displayed in a uniform orange color, i.e., large mineral deposit locations (**e**). Legend abbreviations for resource maps (**a,c,g**) are as follows: watts per square meter ( $\text{W}/\text{m}^2$ ), billion barrels of oil equivalent (BBOE), and tons per hectare ( $\text{t}/\text{ha}$ ).

be used in basic binary overlay assessments<sup>32</sup>, they cannot be used in a gradient spatial analysis that differentiates among areas likely to undergo varying levels of development growth by multiple sectors in the near term.

In addition to elucidating potential individual sector expansion patterns, these DPs can be combined to produce a cumulative development pressure metric at regional or global scales. While each DP is sector specific, the relative index value is a measurement of development suitability based on multiple criteria on resource yield potential and development feasibility. Combining multiple DPs provides a method for illuminating those lands that are suitable for multiple development sectors and thus have more pressures for being used. Although all DPs have been scaled from 0–1, the distribution of these values may vary across sectors. Thus, to ensure equity across all DP values in a cumulative map, we recommend standardizing or classifying each DP relative to an area of interest (e.g., global, regional, country) prior to this process.

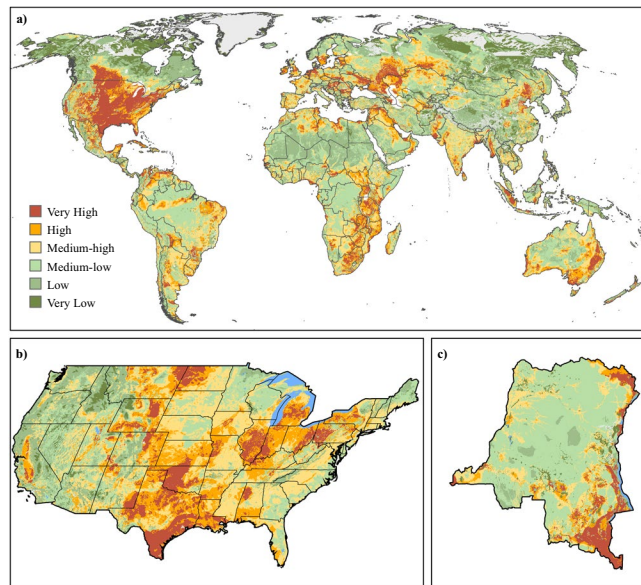


**Fig. 5** Global and regional-level cumulative development maps produced from standardized DPIs. Maps that display (a) global cumulative development potential map based on summing standardized global DPIs, and two regional-level cumulative development potential based on standardizing DPIs at the scale of the (b) United States (US) and (c) Democratic Republic of Congo (DRC). All maps use previously described z-score binning with legend in map (a) also applicable to maps (b,c).

Similar to a cumulative map of marine threats produced by ref.<sup>138</sup>, an additive approach is a simple and an effective way to create a cumulative DPI map. To provide an additive cumulative DPI map in line with the standardization guidelines we recommend above, one can apply globally, standardized z-score values for all continuous DPIs, which are equally-weighted and summed together (Fig. 5a). Such a map allows for countries, states, biomes, and/or ecoregions across the globe to be compared based on cumulative scores (i.e., prior to classification), thereby, identifying areas of varying levels of future development pressure. If the focus is at a more regional or country scale, each continuous DPI can be standardized to that spatial extent before summation. This approach helps to discern high development pressures that are less apparent when DPI values are globally standardized (Fig. 5b,c).

The DPI datasets provide relative measures of development suitability across the most comprehensive set of sectors, thus, serve as important tools that can help anticipate future development patterns at broad spatial scales from multiple sectors. The DPI maps can be combined with existing maps on current land use and land cover (e.g., global Human Modification map<sup>139</sup>, ESA CCI dataset<sup>67</sup>) to help assess opportunity costs and the potential for additional land conversion in a given region. In addition, estimates of production and consumption demand, which influence the likelihood of sector expansion, can also be considered for when quantifying how much potential land may be converted by multiple sectors within a given region (as done by ref.<sup>140</sup>). Together these data with the DPI maps can be used to proactively prioritize regions at a global scale to better plan for near-term tradeoffs among economic development, population growth, and the environment.

### Code Availability

For DPI replication and integration of potential future data updates, we provide via figshare all Python scripts and spatial data necessary to replicate each DPI. Because these DPI scripts require input criteria data totaling 65 GBs in size, we bundled both scripts and data into four compressed files, `DPI_InputsAndCode_Part01-04.zip`<sup>34</sup>. These scripts use ArcPy, a Python module associated with ESRI's ArcGIS Desktop software ([www.esri.com](http://www.esri.com)) and require both the Advance license of this mapping software and an accompanying Spatial Analyst extension license. A *README.pdf* accompanies these zip files and provides all necessary instructions to setup the database and run any of the DPI scripts.

### References

1. Ellis, E. C., Klein Goldewijk, K., Siebert, S., Lightman, D. & Ramankutty, N. Anthropogenic transformation of the biomes, 1700 to 2000. *Glob. Ecol. Biogeogr.* **19**, 598–606 (2010).
2. Foley, J. A. *et al.* Global consequences of land use. *Science* **309**, 570–4 (2005).
3. Steffen, W. *et al.* Planetary boundaries: Guiding human development on a changing planet. *Science* **347**, 1259855 (2015).
4. Ceballos, G., Ehrlich, P. R. & Dirzo, R. Biological annihilation via the ongoing sixth mass extinction signaled by vertebrate population losses and declines. *Proc. Natl. Acad. Sci. USA* **114**, E6089–E6096 (2017).
5. Gerland, P. *et al.* World population stabilization unlikely this century. *Science* **346**, 234–237 (2014).
6. World Bank. *Capital for the Future: Saving and Investment in an Interdependent World*. (World Bank, 2013).
7. DeFries, R. S. *et al.* Planetary opportunities: A social contract for global change science to contribute to a sustainable future. *Bioscience* **62**, 603–606 (2012).

8. Eitelberg, D. A., van Vliet, J. & Verburg, P. H. A review of global potentially available cropland estimates and their consequences for model-based assessments. *Glob. Chang. Biol* **21**, 1236–1248 (2015).
9. Malczewski, J. & Rinner, C. *Multicriteria Decision Analysis in Geographic Information Science*. (Springer Berlin Heidelberg, 2015).
10. Malczewski, J. GIS-based land-use suitability analysis: a critical overview. *Prog. Plann.* **62**, 3–65 (2004).
11. Ramankutty, N., Foley, J. A., Norman, J. & McSweeney, K. The global distribution of cultivable lands: current patterns and sensitivity to possible climate change. *Glob. Ecol. Biogeogr* **11**, 377–392 (2002).
12. Fischer, G. *et al.* *Global Agro-Ecological Zones (GAEZ v3.0) - Model Documentation*. (IIASA, FAO, 2011).
13. Zabel, F., Putzenlechner, B. & Mauser, W. Global agricultural land resources – A high resolution suitability evaluation and its perspectives until 2100 under climate change conditions. *PLoS One* **9**, e107522 (2014).
14. Cai, X., Zhang, X. & Wang, D. Land availability for biofuel production. *Environ. Sci. Technol.* **45**, 334–339 (2011).
15. Field, C. B., Campbell, J. E. & Lobell, D. B. Biomass energy: the scale of the potential resource. *Trends Ecol. Evol.* **23**, 65–72 (2008).
16. Lambin, E. F. *et al.* Estimating the world's potentially available cropland using a bottom-up approach. *Glob. Environ. Chang* **23**, 892–901 (2013).
17. Lu, X., McElroy, M. B. & Kiviluoma, J. Global potential for wind-generated electricity. *Proc. Natl. Acad. Sci. USA* **106**, 10933–8 (2009).
18. Hoes, O. A. C. *et al.* Systematic high-resolution assessment of global hydropower potential. *PLoS One* **12**, e0171844 (2017).
19. Zhou, Y. *et al.* A comprehensive view of global potential for hydro-generated electricity. *Energy Environ. Sci.* **8**, 2622–2633 (2015).
20. Oakleaf, J. R. *et al.* A world at risk: Aggregating development trends to forecast global habitat conversion. *PLoS One* **10**, e0138334 (2015).
21. Köberle, A. C., Gernaat, D. E. H. J. & van Vuuren, D. P. Assessing current and future techno-economic potential of concentrated solar power and photovoltaic electricity generation. *Energy* **89**, 739–756 (2015).
22. Dai, H., Silva Herran, D., Fujimori, S. & Masui, T. Key factors affecting long-term penetration of global onshore wind energy integrating top-down and bottom-up approaches. *Renew. Energy* **85**, 19–30 (2016).
23. Silva Herran, D., Dai, H., Fujimori, S. & Masui, T. Global assessment of onshore wind power resources considering the distance to urban areas. *Energy Policy* **91**, 75–86 (2016).
24. Zhou, Y., Luckow, P., Smith, S. J. & Clarke, L. Evaluation of global onshore wind energy potential and generation costs. *Environ. Sci. Technol.* **46**, 7857–7864 (2012).
25. Bosch, J., Staffell, I. & Hawkes, A. D. Temporally-explicit and spatially-resolved global onshore wind energy potentials. *Energy* **131**, 207–217 (2017).
26. Deng, Y. Y. *et al.* Quantifying a realistic, worldwide wind and solar electricity supply. *Glob. Environ. Chang.* **31**, 239–252 (2015).
27. Eureka, K. *et al.* An improved global wind resource estimate for integrated assessment models. *Energy Econ.* **64**, 522–567 (2017).
28. Singer, D. A., Berver, V. I. & Moring, B. *Porphyry Copper Deposits of the World: Database and Grade and Tonnage Models, 2008*. Open-File Report 2008–1155 (U.S. Geological Survey, 2008).
29. Cox, D. P., Lindsey, D. A., Singer, D. A., Moring, B. C. & Diggles, M. F. *Sediment-Hosted Copper Deposits of the World: Deposit Models and Database*. Open-File Report 03–107 (U.S. Geological Survey, 2007).
30. Schmoker, J. W. & Klett, T. R. *US Geological Survey Assessment Concepts for Conventional Petroleum Accumulations*. (U.S. Geological Survey, 2005).
31. US Energy Information Administration. *World Shale Resource Assessments*, <https://www.eia.gov/analysis/studies/worldshalegas/> (2015).
32. Butt, N. *et al.* Conservation. *Biodiversity risks from fossil fuel extraction*. *Science* **342**, 425–6 (2013).
33. Harfoot, M. B. J. *et al.* Present and future biodiversity risks from fossil fuel exploitation. *Conserv. Lett.* **11**, e12448 (2018).
34. Oakleaf, J. R. *et al.* Global development potential indices for renewable energy, fossil fuels, mining and agriculture sectors. *figshare*, <https://doi.org/10.6084/m9.figshare.c.4249532> (2019).
35. Eastman, R., Jin, W., Kyem, P. & Toledano, J. Raster procedures for multi-criteria/multi-objective decisions. *Photogramm. Eng. Remote Sens.* **61**, 503–511 (1995).
36. Saaty, R. W. The analytic hierarchy process—what it is and how it is used. *Math. Model.* **9**, 161–176 (1987).
37. Saaty, T. L. *The Analytic Hierarchy Process*. (McGraw-Hill, 1980).
38. Saaty, T. L. How to make a decision: The analytic hierarchy process. *Eur. J. Oper. Res.* **48**, 9–26 (1990).
39. Grandmont, K., Cardille, J. A., Fortier, D. & Giberyen, T. Assessing land suitability for residential development in permafrost regions: A multi-criteria approach to land-use planning in Northern Quebec, Canada. *J. Environ. Assess. Policy Manag* **14**, 1250003 (2012).
40. Chen, Y., Yu, J. & Khan, S. The spatial framework for weight sensitivity analysis in AHP-based multi-criteria decision making. *Environ. Model. Softw* **48**, 129–140 (2013).
41. Adem Esmail, B. & Geneletti, D. Multi-criteria decision analysis for nature conservation: A review of 20 years of applications. *Methods Ecol. Evol* **9**, 42–53 (2018).
42. Tegou, L.-I., Polatidis, H. & Haralambopoulos, D. A. Environmental management framework for wind farm siting: Methodology and case study. *J. Environ. Manage.* **91**, 2134–2147 (2010).
43. Aragonés-Beltrán, P., Chaparro-González, F., Pastor-Ferrando, J. P., Pla-Rubio, A. & An, A. H. P. Analytic Hierarchy Process)/ANP (Analytic Network Process)-based multi-criteria decision approach for the selection of solar-thermal power plant investment projects. *Energy* **66**, 222–238 (2014).
44. Jangid, J. *et al.* Potential zones identification for harvesting wind energy resources in desert region of India – A multi criteria evaluation approach using remote sensing and GIS. *Renewable and Sustainable Energy Reviews* **65**, 1–10 (2016).
45. Janke, J. R. Multicriteria GIS modeling of wind and solar farms in Colorado. *Renew. Energy* **35**, 2228–2234 (2010).
46. Effat, H. & Effat, H. A. Selection of potential sites for solar energy farms in Ismailia Governorate, Egypt using SRTM and multicriteria analysis. *Int. J. Adv. Remote Sens. GIS* **2**, 205–220 (2013).
47. Blachowski, J. Methodology for assessment of the accessibility of a brown coal deposit with Analytical Hierarchy Process and Weighted Linear Combination. *Environ. Earth Sci.* **74**, 4119–4131 (2015).
48. Mohammed, A. & Alshayef, M. Integration based GIS weighted linear combination (WLC) model for delineation hydrocarbon potential zones in Ayad Area (Yemen) using analytic hierarchy process (AHP) technique. *SSRG Int. J. Geoinformatics Geol. Sci* **4**, 1–5 (2017).
49. Baranzelli, C. *et al.* Scenarios for shale gas development and their related land use impacts in the Baltic Basin, Northern Poland. *Energy Policy* **84**, 80–95 (2015).
50. Pazand, K., Hezarkhani, A., Ataei, M. & Ghanbari, Y. Combining AHP with GIS for predictive Cu porphyry potential mapping: A case study in Ahar Area (NW, Iran). *Nat. Resour. Res* **20**, 251–262 (2011).
51. Zolekar, R. B. & Bhagat, V. S. Multi-criteria land suitability analysis for agriculture in hilly zone: Remote sensing and GIS approach. *Comput. Electron. Agric.* **118**, 300–321 (2015).
52. Wulandari, W. S., Darusman, D., Kusmana, C. & Land, W. suitability analysis of biodiesel crop Kemiri Sunan (*Reutealis trisperma* (Blanco) Airy Shaw) in the province of West Java, Indonesia. *J. Environ. Earth Sci* **4**, 27–37 (2014).
53. Khoi, D. D. & Murayama, Y. Delineation of suitable cropland areas using a GIS based multi-criteria evaluation approach in the tam Dao national park region, Vietnam. *Sustainability* **2**, 2024–2043 (2010).

54. van Vliet, J., Eitelberg, D. A. & Verburg, P. H. A global analysis of land take in cropland areas and production displacement from urbanization. *Glob. Environ. Chang* **43**, 107–115 (2017).
55. Hermann, S., Miketa, A. & Fichaux, N. *Estimating the Renewable Energy Potential in Africa*. (IREA, 2014).
56. Wu, G. C. *et al.* Strategic siting and regional grid interconnections key to low-carbon futures in African countries. *Proc. Natl. Acad. Sci. USA* **114**, E3004–E3012 (2017).
57. Wu, G. C., Deshmukh, R., Ndhlukula, K., Radojicic, T. & Reilly, J. *Renewable Energy Zones for the Africa Clean Energy Corridor*. (IRENA, 2015).
58. He, G. & Kammen, D. M. Where, when and how much solar is available? A provincial-scale solar resource assessment for China. *Renew. Energy* **85**, 74–82 (2016).
59. Lopez, A., Roberts, B., Heimiller, D., Blair, N. & Porro, G. *U.S. Renewable Energy Technical Potentials: A GIS-Based Analysis*. (NREL, 2012).
60. He, G. & Kammen, D. M. Where, when and how much wind is available? A provincial-scale wind resource assessment for China. *Energy Policy* **74**, 116–122 (2014).
61. Hernandez, R. R., Hoffacker, M. K., Murphy-Mariscal, M. L., Wu, G. C. & Allen, M. F. Solar energy development impacts on land cover change and protected areas. *Proc. Natl. Acad. Sci. USA* **112**, 13579–84 (2015).
62. Miller, A. & Li, R. A geospatial approach for prioritizing wind farm development in Northeast Nebraska, USA. *ISPRS Int. J. Geo-Information* **3**, 968–979 (2014).
63. Elsheikh, R. *et al.* Agriculture Land Suitability Evaluator (ALSE): A decision and planning support tool for tropical and subtropical crops. *Comput. Electron. Agric.* **93**, 98–110 (2013).
64. Gorsevski, P. V. *et al.* A group-based spatial decision support system for wind farm site selection in Northwest Ohio. *Energy Policy* **55**, 374–385 (2013).
65. Clifton, J. & Boruff, B. J. Assessing the potential for concentrated solar power development in rural Australia. *Energy Policy* **38**, 5272–5280 (2010).
66. Brewer, J., Ames, D. P., Solan, D., Lee, R. & Carlisle, J. Using GIS analytics and social preference data to evaluate utility-scale solar power site suitability. *Renew. Energy* **81**, 825–836 (2015).
67. CCI-LC consortium. *Climate Change Initiative - Land Cover database*, <http://maps.elie.ucl.ac.be/CCI/viewer/download.php> (2017).
68. Tesfaw, A. T. *et al.* Land-use and land-cover change shape the sustainability and impacts of protected areas. *Proc. Natl. Acad. Sci. USA* **115**, 2084–2089 (2018).
69. Howell, D. C. *Statistical Methods for Psychology*. (Cengage Learning, 2013).
70. Tabachnick, B. G. & Fidell, L. S. *Using Multivariate Statistics*. (Pearson Education, 2012).
71. Singer, D. A. Mineral deposit densities for estimating mineral resources. *Math. Geosci.* **40**, 33–46 (2008).
72. Singer, D. A. & Kouda, R. Probabilistic Estimates of number of undiscovered deposits and their total tonnages in permissive tracts using deposit densities. *Nat. Resour. Res* **20**, 89–93 (2011).
73. Silverman, B. W. *Density Estimation for Statistics and Data Analysis*. (Routledge, 2018).
74. Cassard, D. *et al.* ProMine Mineral Databases: New Tools to Assess Primary and Secondary Mineral Resources in Europe. In *3D, 4D and Predictive Modelling of Major Mineral Belts in Europe* (ed. Weihed, P.) 9–58 (Springer, Cham, 2015).
75. Lisitsin, V. *Mineral prospectivity analysis and quantitative resource assessments for regional exploration targeting: development of effective integration models and practical applications*. (The University of Western Australia, 2015).
76. Cassidy, E. S., West, P. C., Gerber, J. S. & Foley, J. A. Redefining agricultural yields: from tonnes to people nourished per hectare. *Environ. Res. Lett.* **8**, 034015 (2013).
77. International Energy Agency. *Technology Roadmap: Biofuels for Transport*. (IEA, 2011).
78. Fargione, J. E., Plevin, R. J. & Hill, J. D. The ecological impact of biofuels. *Annu. Rev. Ecol. Evol. Syst.* **41**, 351–377 (2010).
79. Mueller, N. D. *et al.* Closing yield gaps through nutrient and water management. *Nature* **490**, 254–257 (2012).
80. The Mining Association of Canada. *Levelling the Playing Field Supporting Mineral Exploration and Mining in Remote and Northern Canada*. (The Mining Association of Canada, 2015).
81. Saaty, T. L. & Vargas, L. G. *Models, Methods, Concepts, and Applications of the Analytic Hierarchy Process*. 175, (Springer Science & Business Media, 2012).
82. IREA. *Renewable Power Generation Costs in 2014*. (IRENA, 2015).
83. Finer, M. *et al.* Future of oil and gas development in the western Amazon. *Environ. Res. Lett.* **10**, 024003 (2015).
84. Henderson, J. & Loe, J. *The Prospects and Challenges for Arctic Oil Development*. (The Oxford Institute for Energy Studies, 2014).
85. US Energy Information Administration. *Trends in U.S. Oil and Natural Gas Upstream Costs*. (US EIA, 2016).
86. Petak, K. *et al.* *U.S. Oil and Gas Infrastructure Investment Through 2035*. (API, 2017).
87. Finer, M., Jenkins, C. N. & Powers, B. Potential of best practice to reduce impacts from oil and gas projects in the amazon. *PLoS One* **8**, e63022 (2013).
88. Ríos-Mercado, R. Z. & Borraz-Sánchez, C. Optimization problems in natural gas transportation systems: A state-of-the-art review. *Appl. Energy* **147**, 536–555 (2015).
89. US Department of Energy. *Impact of Increasing US LNG Exports*. (DOE, 2015).
90. Holditch, S. A. Unconventional oil and gas resource development – Let’s do it right. *J. Unconv. Oil Gas Resour* **1–2**, 2–8 (2013).
91. Schaffartzik, A., Mayer, A., Eisenmenger, N. & Krausmann, F. Global patterns of metal extractivism, 1950–2010: Providing the bones for the industrial society’s skeleton. *Ecol. Econ.* **122**, 101–110 (2016).
92. Kogel, J. E., Trivedi, N. & Herpfer, M. A. Measuring sustainable development in industrial minerals mining. *Int. J. Min. Miner. Eng.* **5**, 4–18 (2014).
93. Cotrell, J. *et al.* *Analysis of Transportation and Logistics Challenges Affecting the Deployment of Larger Wind Turbines: Summary of Results*. (NREL, 2014).
94. Robinson, G. R. & Menzie, W. D. *Economic Filters for Evaluation Porphyry Copper Deposit Respire Assess, emts Isomg Grade-Tonage Deposit Models, with Examples from the US Geological Survey Global Mineral Resource Assessment*. (U.S. Geological Survey, 2014).
95. Choi, Y. & Song, J. Review of photovoltaic and wind power systems utilized in the mining industry. *Renew. Sustain. Energy Rev.* **75**, 1386–1391 (2017).
96. Blachowski, J. Spatial analysis of the mining and transport of rock minerals (aggregates) in the context of regional development. *Environ. Earth Sci.* **71**, 1327–1338 (2014).
97. Karakas, A. & Turner, K. Aggregate supply and demand modeling using GIS methods for the front range urban corridor, Colorado. *Comput. Geosci.* **30**, 579–590 (2004).
98. Chamberlin, J., Jayne, T. S. & Headey, D. Scarcity amidst abundance? Reassessing the potential for cropland expansion in Africa. *Food Policy* **48**, 51–65 (2014).
99. Villoria, N. B. & Liu, J. Using spatially explicit data to improve our understanding of land supply responses: An application to the cropland effects of global sustainable irrigation in the Americas. *Land use policy* **75**, 411–419 (2018).
100. Keys, E. & McConnell, W. J. Global change and the intensification of agriculture in the tropics. *Glob. Environ. Chang* **15**, 320–337 (2005).
101. Strager, M. P. *et al.* Combining a spatial model and demand forecasts to map future surface coal mining in Appalachia. *PLoS One* **10**, e0128813 (2015).

102. Rutledge, D. Estimating long-term world coal production with logit and probit transforms. *Int. J. Coal Geol.* **85**, 23–33 (2011).
103. U.S. Energy Information Administration. *Annual Coal Distribution Report 2016*. (US EIA, 2017).
104. Kumar, Y. *et al.* Wind energy: Trends and enabling technologies. *Renew. Sustain. Energy Rev.* **53**, 209–224 (2016).
105. Mutchek, M., Cooney, G., Pickenpugh, G., Marriott, J. & Skone, T. Understanding the contribution of mining and transportation to the total life cycle impacts of coal exported from the United States. *Energies* **9**, 559 (2016).
106. Lark, T. J., Meghan Salmon, J. & Gibbs, H. K. Cropland expansion outpaces agricultural and biofuel policies in the United States. *Environ. Res. Lett.* **10**, 044003 (2015).
107. Robinson, G. R., Kapo, K. E. & Raines, G. L. A. GIS analysis to evaluate areas suitable for crushed stone aggregate quarries in New England, USA. *Nat. Resour. Res.* **13**, 143–159 (2004).
108. Luo, G., Li, Y., Tang, W. & Wei, X. Wind curtailment of China's wind power operation: Evolution, causes and solutions. *Renew. Sustain. Energy Rev.* **53**, 1190–1201 (2016).
109. Jager, H. I., Efraymson, R. A., Opperman, J. J. & Kelly, M. R. Spatial design principles for sustainable hydropower development in river basins. *Renew. Sustain. Energy Rev.* **45**, 808–816 (2015).
110. Miao, C., Borthwick, A., Liu, H. & Liu, J. China's policy on dams at the crossroads: Removal or further construction? *Water* **7**, 2349–2357 (2015).
111. Kucukali, S. Risk assessment of river-type hydropower plants using fuzzy logic approach. *Energy Policy* **39**, 6683–6688 (2011).
112. Paish, O. Small hydro power: technology and current status. *Renew. Sustain. Energy Rev.* **6**, 537–556 (2002).
113. Bleiwas, D. I. *Estimates of Electricity Requirements for the Recovery of Mineral Commodities, with Examples Applied to Sub-Saharan Africa*. (U.S. Geological Survey, 2011).
114. Halpern, B. S. *et al.* A global map of human impact on marine ecosystems. *Science* **319**, 948–952 (2008).
115. Chen, Y., Yu, J. & Khan, S. Spatial sensitivity analysis of multi-criteria weights in GIS-based land suitability evaluation. *Environ. Model. Softw.* **25**, 1582–1591 (2010).
116. Ligmann-Zielinska, A. & Jankowski, P. Spatially-explicit integrated uncertainty and sensitivity analysis of criteria weights in multicriteria land suitability evaluation. *Environ. Model. Softw.* **57**, 235–247 (2014).
117. Quinn, B., Schiel, K. & Caruso, G. Mapping uncertainty from multi-criteria analysis of land development suitability, the case of Howth, Dublin. *J. Maps* **11**, 487–495 (2015).
118. Shokati, B. & Feizizadeh, B. Sensitivity and uncertainty analysis of agro-ecological modeling for saffron plant cultivation using GIS spatial decision-making methods. *J. Environ. Plan. Manag.* **62**, 517–533 (2018).
119. Paul, M. C. *et al.* Quantitative assessment of a spatial multicriteria model for highly pathogenic avian influenza H5N1 in Thailand, and application in Cambodia. *Sci. Rep.* **6**, 31096 (2016).
120. McIntosh, B. S. *et al.* Environmental decision support systems (EDSS) development – Challenges and best practices. *Environ. Model. Softw.* **26**, 1389–1402 (2011).
121. Dahri, N. & Abida, H. Monte Carlo simulation-aided analytical hierarchy process (AHP) for flood susceptibility mapping in Gabes Basin (southeastern Tunisia). *Environ. Earth Sci* **76**, 302 (2017).
122. Feizizadeh, B., Jankowski, P. & Blaschke, T. A GIS based spatially-explicit sensitivity and uncertainty analysis approach for multi-criteria decision analysis. *Comput. Geosci.* **64**, 81–95 (2014).
123. ABB Enterprise Software. *EV Energy Map - Wind and Solar Power Plants.*, <http://energymarketintel.com/solutions-energy-market-intelligence/market-data/velocity-suite/ev-energy-map-2/> (2018).
124. Zarfl, C., Lumsdon, A. E., Berlekamp, J., Tydecks, L. & Tockner, K. A global boom in hydropower dam construction. *Aquat. Sci.* **77**, 161–170 (2014).
125. Mainer, D. J. *et al.* *Summary of science, activities, programs, and policies that influence the rangewide conservation of Greater Sage-Grouse (Centrocercus urophasianus)*. *Open-File Report 2013–1098* (U.S. Geological Survey, 2013).
126. US DOI - Office of Surface Mining Reclamation and Enforcement. *Currently Permitted Surface CMOs.*, <http://geomine.osmre.gov/> (2018).
127. Yu, Z. & Lu, C. Historical cropland expansion and abandonment in the continental U.S. during 1850 to 2016. *Glob. Ecol. Biogeogr.* **27**, 322–333 (2018).
128. Ong, S., Campbell, C., Denholm, P., Margolis, R. & Heath, G. *Land-Use Requirements for Solar Power Plants in the United States*. (NREL, 2013).
129. Denholm, P., Hand, M., Jackson, M. & Ong, S. *Land-use requirements of modern wind power plants in the United States*. (NREL, 2009).
130. Demirbaş, A. Global renewable energy resources. *Energy Sources, Part A Recover. Util. Environ. Eff.* **28**, 779–792 (2006).
131. Kiesecker, J. M. & Naugle, D. E. *Energy Sprawl Solutions: Balancing Global Development and Conservation*. (Island Press, 2017).
132. Verburg, P. H., van Asselen, S., van der Zanden, E. H. & Stehfest, E. The representation of landscapes in global scale assessments of environmental change. *Landsc. Ecol.* **28**, 1067–1080 (2013).
133. Prestele, R. *et al.* Hotspots of uncertainty in land-use and land-cover change projections: A global-scale model comparison. *Glob. Chang. Biol.* **22**, 3967–3983 (2016).
134. Wuebbles, D. J. *et al.* Executive summary. In *Climate Science Special Report: Fourth National Climate Assessment* (eds Wuebbles, D. J. *et al.*) 12–34 (U.S. Global Change Reserch Program, 2017).
135. IPCC. Summary for Policymakers. In *Global Warming of 1.5 °C. An IPCC Special Report on the impacts of global warming of 1.5 °C above pre-industrial levels and related global greenhouse gas emission pathways, in the context of strengthening the global response to the threat of climate change*. (eds Masson-Delmotte, V. *et al.*) 32 (World Meteorological Organization, 2018).
136. Openshaw, S. & Taylor, P. J. The modifiable areal unit problem. In *Quantitative Geography: A British View* (eds Wrigley, N. & Bennett, R. J.) 60–70 (Routledge and Kegan Paul, 1981).
137. Schuurman, N., Bell, N., Dunn, J. R. & Oliver, L. Deprivation indices, population health and geography: An evaluation of the spatial effectiveness of indices at multiple scales. *J. Urban Heal* **84**, 591–603 (2007).
138. Halpern, B. S. *et al.* Spatial and temporal changes in cumulative human impacts on the world's ocean. *Nat. Commun.* **6**, 7615 (2015).
139. Kennedy, C. M., Oakleaf, J. R., Theobald, D. M., Baruch-Mordo, S. & Kiesecker, J. Managing the middle: A shift in conservation priorities based on the global human modification gradient. *Glob. Chang. Biol.* **25**, 811–826 (2019).
140. Tallis, H. M. *et al.* An attainable global vision for conservation and human well-being. *Front. Ecol. Environ.* **16**, 563–570 (2018).
141. VAISALA. *Global Solar Dataset 3 km with units in W/m<sup>2</sup>/day*, <http://geocatalog.webservice-energy.org/geonetwork/srv/eng/metadata.show?uuid=204528bb5b72311f3d656d8e93209866b1355218> (2016).
142. FAO & IIASA. *Harmonized World Soil Database v1.2*, <http://www.fao.org/soils-portal/soil-survey/soil-maps-and-databases/harmonized-world-soil-database-v12/en/> (2012).
143. Latham, J., Cumani, R., Rosati, I. & Bloise, M. *Global land cover share (GLC\_SHARE) database beta-release version 1.0*, <http://www.fao.org/geonetwork/srv/en/main.home?uuid=ba4526fd-cdbf-4028-a1bd-5a559c4bf38> (2013).
144. National Renewable Energy Laboratory. *Concentrating Solar Power Projects*, <https://solarpaces.nrel.gov/> (2016).
145. VAISALA. *Global Wind Dataset 5km onshore wind speed at 80m height units in m/s*, <http://geocatalog.webservice-energy.org/geonetwork/srv/eng/metadata.show?uuid=36bf7290dbb842e4e3b5541ffe8197db5320b90> (2016).
146. EROS Data Center. *Global 30 Arc-Second Elevation Data Set*, <https://lta.cr.usgs.gov/GTOPO30> (U.S. Geological Survey, 1996).

147. Islam, M. R., Mekhilef, S. & Saidur, R. Progress and recent trends of wind energy technology. *Renew. Sustain. Energy Rev.* **21**, 456–468 (2013).
148. Diffendorfer, J. E., Compton, R., Kramer, L. A., Ancona, Z. & Norton, D. *Onshore industrial wind turbine locations for the United States* (U.S. Geological Survey, 2014).
149. Lehner, B. *et al.* High-resolution mapping of the world's reservoirs and dams for sustainable river-flow management. *Front. Ecol. Environ.* **9**, 494–502 (2011).
150. Brownfield, M. *et al.* *Coal Quality and Resources of the Former Soviet Union - An ArcView Project*. Open-File Report 02–104 (U.S. Geological Survey, 2001).
151. Ewers, G. R., Evens, N., Hazell, M. & Kilgour, B. *Geoscience Australia - Operating Mines of Australia*, <http://www.australianminesatlas.gov.au/mapping/metadata.html#ozmin> (2015).
152. Tewalt, S. J., Kinney, S. A. & Merrill, M. D. *GIS representation of coal-bearing areas in North, Central, and South America*. Open-File Report 2008–1257 (U.S. Geological Survey, 2008).
153. Trippi, M. H. & Belkin, H. E. *USGS compilation of geographic information system (GIS) data of coal mines and coal-bearing areas in Mongolia*. Open-File Report 2015–1144 (U.S. Geological Survey, 2015).
154. Trippi, M. H., Belkin, H. E., Dai, S., Tewalt, S. J. & Chou, C. *USGS Compilation of Geographic Information System (GIS) Data Representing Coal Mines and Coal-Bearing Areas in China*. Open-File Report 2014–1219 (U.S. Geological Survey, 2014).
155. Trippi, M. H. & Tewalt, S. J. *Geographic information system (GIS) representation of coal-bearing areas in India and Bangladesh*. Open-File Report 2011–1296 (U.S. Geological Survey, 2011).
156. U.S. Energy Information Administration. *Active US Coal Mines*, [https://www.eia.gov/maps/layer\\_info-m.php](https://www.eia.gov/maps/layer_info-m.php) (2016).
157. U.S. Geological Survey. *Mineral operations outside the United States*, <https://mrdata.usgs.gov/mineral-operations/> (2010).
158. U.S. Geological Survey. *USGS 2012 World Assessment of Undiscovered Oil and Gas Resources*, <http://pubs.usgs.gov/dds/dds-069/dds-069-ff/> (2012).
159. U.S. Geological Survey. *World Petroleum Assessment 2000*, <http://pubs.usgs.gov/dds/dds-060/> (2000).
160. U.S. Geological Survey. *National Oil and Gas Assessment*, <http://energy.usgs.gov/OilGas/AssessmentsData/NationalOilGasAssessment/AssessmentUpdates.aspx> (2012).
161. Geoscience Australia. *Australian Energy Resource Assessment*. (Geoscience Australia, 2014).
162. U.S. Energy Information Administration. *Technically Recoverable Shale Oil and Shale Gas Resources: An Assessment of 137 Shale Formations in 41 Countries Outside the United States*. (U.S. EIA, 2013).
163. U.S. Geological Survey. *U.S. Geological Survey assessments of continuous (unconventional) oil and gas resources, 2000 to 2011*. Digital Data Series DDS-69-MM (2015).
164. U.S. Geological Survey. *USGS National Assessment of Oil and Gas Project - Shale Gas Assessment Units*, <https://catalog.data.gov/dataset/usgs-national-assessment-of-oil-and-gas-project-shale-gas-assessment-units> (2013).
165. Gilmore, E., Gleditsch, N. P., Lujala, P. & Rod, J. K. Conflict diamonds: A new dataset. *Confl. Manag. Peace Sci* **22**, 257–292 (2005).
166. Kirkham, R. V. & Dunne, K. P. E. *World porphyry and porphyry-related deposit database*, <https://doi.org/10.4095/297319> (2015).
167. Kirkham, R. V., Carriere, J. J., Rafer, A. B. & Born, P. *World sediment-hosted copper deposit database*, <https://doi.org/10.4095/296422> (2015).
168. Gandhi, S. *World Fe Oxide +/- Cu-Au-U (IOCG) deposit database*, <https://doi.org/10.4095/296424> (Natural Resources Canada, 2015).
169. Orris, G. J. *et al.* *Potash—A global overview of evaporite-related potash resources, including spatial databases of deposits, occurrences, and permissive tracts*. Scientific Investigations Report 2010–5090–S (U.S. Geological Survey, 2014).
170. Kirkham, R. V. & Rafer, A. B. *Selected World Mineral Deposits Database*. <https://doi.org/10.4095/214766> (2003).
171. Schulz, K. J. & Briske, J. A. *Major mineral deposits of the world*. Open-File Report 2005–1294 (U.S. Geological Survey, 2005).
172. U.S. Geological Survey. *Mineral Resources Data System (MRDS)*, <http://mrdata.usgs.gov/mrds/> (2005).
173. Blachowski, J. GIS-based spatial assessment of rock minerals mining - a case study of the Lower Silesia Region (SW Poland). *Min. Sci.* **22**, 7–22 (2015).
174. Ray, D. K., Ramankutty, N., Mueller, N. D., West, P. C. & Foley, J. A. Recent patterns of crop yield growth and stagnation. *Nat. Commun.* **3**, 1293 (2012).
175. Hijmans, R. J., Cameron, S. E., Parra, J. L., Jones, P. G. & Jarvis, A. Very high resolution interpolated climate surfaces for global land areas. *Int. J. Climatol.* **25**, 1965–1978 (2005).
176. Blyth, E. *et al.* Creation of the WATCH Forcing Data and its use to assess global and regional reference crop evaporation over land during the twentieth century. *J. Hydrometeorol.* **12**, 823–848 (2011).
177. Batjes, N. H. *ISRIC-WISE derived soil properties on a 5 by 5 arc-minutes global grid (ver 1.2)*, <https://data.isric.org/geonetwork/srv/eng/catalog.search#/metadata/82f3d6b0-a045-4fe2-b960-6d05bc1f37c0> (2012).
178. Siebert, S. *et al.* Development and validation of the global map of irrigation areas. *Hydrol. Earth Syst. Sci. Discuss.* **2**, 1299–1327 (2005).
179. Hazeu, G. *et al.* A unified cropland layer at 250 m for global agriculture monitoring. *Data* **1**, 3 (2016).
180. Johnson, J. A., Runge, C. F., Senauer, B., Foley, J. & Polasky, S. Global agriculture and carbon trade-offs. *Proc. Natl. Acad. Sci. USA* **111**, 12342–7 (2014).
181. Schneider, A., Friedl, M. & Potere, D. A new map of global urban extent from MODIS data. *Environ. Res. Lett.* **4** (2009).
182. National Geospatial Agency. *Digital Chart of the World*, <http://gis-lab.info/qa/vmap0-eng.html> (2000).
183. National Geospatial-Intelligence Agency. *World Port Index*, [http://msi.nga.mil/NGAPortal/MSI.portal?\\_nfpb=true&\\_pageLabel=msi\\_portal\\_page\\_62&pubCode=0015](http://msi.nga.mil/NGAPortal/MSI.portal?_nfpb=true&_pageLabel=msi_portal_page_62&pubCode=0015) (2016).
184. Small, C., Elvidge, C. D., Balk, D. & Montgomery, M. Spatial scaling of stable night lights. *Remote Sens. Environ.* **115**, 269–280 (2011).
185. Ummell, K. *CARMA revisited: an updated database of carbon dioxide emissions from power plants worldwide*, <http://carma.org/dig/> (2012).
186. NOAA National Centers for Environmental Information. *Version 4 DMSP-OLS, Stable Nighttime Lights - 2013*, <http://ngdc.noaa.gov/eog/dmsp/downloadV4composites.html> (2013).
187. Center for International Earth Science Information Network - CIESIN. *Gridded Population of the World, Verstio 4 (GPWv4)*, <https://doi.org/10.7927/H4X63JVC> (2016).
188. Bureau of the Census - Department of Commerce. *Qualifying Urban Areas for the 2010 Census*. **77**, 18652–18669 (2012).
189. Natural Earth. *Populated Places*, <http://www.naturalearthdata.com/downloads/10m-cultural-vectors/10m-populated-places/> (2012).
190. European Space Agency. *Land Cover Map - 2010 epoch*, <http://maps.elie.ucl.ac.be/CCI/viewer/download.php> (2014).
191. Lujala, P., Rod, J. K. & Thieme, N. Fighting over oil: Introducing a new dataset. *Confl. Manag. Peace Sci* **24**, 239–256 (2007).
192. Baugh, K., Elvidge, C. D., Ghosh, T. & Ziskin, D. Development of a 2009 stable lights product using DMSP-OLS data. *Proc. Asia-Pacific Adv. Netw.* **30**, 114 (2012).
193. Elvidge, C., Ghosh, T., Hsu, F.-C., Baugh, K. & Zhizhin, M. Methods for global survey of natural gas glaring from visible infrared imaging radiometer suite data. *Energies* **9**, 14 (2015).
194. NOAA National Centers for Environmental Information. *NOAA VIIRS Nightfire Data - Prerun V2.1. Flares Only*, [https://ngdc.noaa.gov/eog/viirs/download\\_viirs\\_flares\\_only.html](https://ngdc.noaa.gov/eog/viirs/download_viirs_flares_only.html) (2017).



195. Weiss, D. J. *et al.* A global map of travel time to cities to assess inequalities in accessibility in 2015. *Nature* **553**, 333–336 (2018).
196. Verburg, P. H., Ellis, E. C. & Letourneau, A. A global assessment of market accessibility and market influence for global environmental change studies. *Environ. Res. Lett.* **6**, 034019 (2011).
197. Robinson, G. R. Jr. & Brown, W. M. *Sociocultural Dimensions of Supply and Demand for Natural Aggregate— Examples from the Mid-Atlantic Region, United States.* (U.S. Geological Survey, 2002).
198. Hyder, Z., Ripepi, N. S. & Karmis, M. E. A life cycle comparison of greenhouse emissions for power generation from coal mining and underground coal gasification. *Mitig. Adapt. Strateg. Glob. Chang* **21**, 515–546 (2016).
199. Kosfeld, R., Eckey, H.-F. & Lauridsen, J. Spatial point pattern analysis and industry concentration. *Ann. Reg. Sci.* **47**, 311–328 (2011).

## Acknowledgements

This work was supported by The Nature Conservancy, Anne Ray Charitable Trust, MacArthur Foundation, The Robertson Foundation, donation from Roy Vagelos, and the 3M Foundation. We thank Colorado State University Geospatial Centroid for their digitizing and tabular data development. We also thank all data providers who contributed open source data used in our analysis, thereby providing a better understanding of the world we live in. Special thanks to Phil Connors who mentored us through the constant effort of improving this analysis and led by example on how to eventually finish a lengthy project.

## Author Contributions

J.R.O., C.M.K., S.B.M., J.S.G. and J.K. conceived and designed the study; J.R.O., S.B.M. and J.S.G. aggregated input data and conducted analyses; J.R.O. conducted model uncertainty, sensitivity, and validation analyses; J.R.O., C.M.K. and S.B.M. produced the figures and tables; J.R.O., C.M.K., S.B.M., J.A.J., J.S.G., P.C.W. and J.K. interpreted the results; J.R.O., C.M.K., S.B.M., and J.K. designed and wrote the paper; J.R.O., C.M.K., S.B.M., J.A.J., J.S.G., P.C.W. and J.K. revised the paper.

## Additional Information

**Supplementary information** is available for this paper at <https://doi.org/10.1038/s41597-019-0084-8>.

**Competing Interests:** The authors declare no competing interests.

**Publisher's note:** Springer Nature remains neutral with regard to jurisdictional claims in published maps and institutional affiliations.



**Open Access** This article is licensed under a Creative Commons Attribution 4.0 International License, which permits use, sharing, adaptation, distribution and reproduction in any medium or format, as long as you give appropriate credit to the original author(s) and the source, provide a link to the Creative Commons license, and indicate if changes were made. The images or other third party material in this article are included in the article's Creative Commons license, unless indicated otherwise in a credit line to the material. If material is not included in the article's Creative Commons license and your intended use is not permitted by statutory regulation or exceeds the permitted use, you will need to obtain permission directly from the copyright holder. To view a copy of this license, visit <http://creativecommons.org/licenses/by/4.0/>.

The Creative Commons Public Domain Dedication waiver <http://creativecommons.org/publicdomain/zero/1.0/> applies to the metadata files associated with this article.

© The Author(s) 2019